Impact of Levee Axis Adjustment on Flow Variation in Xinsha Island

Wuyi Yu , Hanbin Gu * , Dongxu Wang , Efrain Carpintero Moreno , Jun Zang

Posted Date: 3 March 2026

doi: 10.20944/preprints202603.0241.v1

Keywords: Fuchun river; numerical river flow modelling; levee Adjustment; hydrological impacts

 doi:10.20944/preprints202603.0241.v1

Article

Impact of Levee Axis Adjustment on Flow Variation in Xinsha Island

Wuyi Yu [1], Hanbin Gu [1,*], Dongxu Wang [1], Efrain Carpintero Moreno [2] and Jun Zang [3]

[1] Institute of Hydraulics and Ocean Engineering /School of Civil & Environmental Engineering and Geography Science, Ningbo University, Ningbo 315211, China

[2] Department of Civil Engineering, Ghent University, Technologiepark 60, 9052, Ghent, Belgium

[3] Department of Architecture & Civil Engineering, University of Bath, UK, BA27AY

* Correspondence: hanbin.gu@163.com

Abstract

To analyse impact of levee axis adjustment on flow variation in the Xinsha Island which is located in the middle segment of the Fuchun river waterway in Fuyang, Hangzhou, a two-dimensional river flow model was constructed. In the model steady flow with different return periods and unsteady flow in 20-year period were simulated. Consistent outcomes were obtained under steady and unsteady flow. Results indicated that after the levee axis is adjusted, the longer the return periods, the higher the water level in the southern waterway, with a maximum increase of 0.183 m. Conversely, the northern waterway exhibits a more pronounced water level decrease, with a maximum reduction of 0.128 m. The flow velocity of the southern waterway slows down, and the flow velocity of the northern waterway increases. After the levee axis is adjusted, the flow diversion capacity of the north waterway is effectively enhanced, thereby benefiting flood regulation. These findings provide a sound theoretical basis and well-founded recommendations for adjusting levee axis position and enhancing flood resilience in the Xinsha Island area of the Fuchun River.

Keywords: Fuchun river; numerical river flow modelling; levee Adjustment; hydrological impacts

1. Introduction

China's flood disasters, induced by climate change and extreme weather, are becoming more frequent, affecting larger areas, and intensifying. These floods pose a significant threat to public safety and hinder national economic progress [1–4]. To accurately assess how floods change before and after engineering projects, mathematical modelling is usually essential for simulating the basin numerically, examining changes in hydrological conditions over different return periods [5–8].

Hydrodynamic river flow models essentially resolve the governing physical equations that describe the motion of water bodies under certain initial circumstances to generate essential hydraulic parameters [9–12]. In 1871, French scientist Saint-Venant developed a model utilising a water channel to examine variations in flow mass and energy, introducing the well-known Saint-Venant equations that laid the theoretical groundwork for future hydrodynamic simulation studies [13,14]. In 1938, G.T. McCarthy developed the channel storage equation to forecast downstream flood progression in rivers, leading to the establishment of the Muskingum mathematical model for flood evolution, which has been subject to ongoing refinement and optimisation during its application [15]. From 1952 to 1954, Issaacson et al. developed mathematical models for segments of the Mississippi and Ohio rivers in the United States, simulating flood dynamics [16]. In 1976, Cunge presented several examples of the successful application of an implicit numerical method to flood routing in natural and artificial channels [17]. In 1997, Bernard advanced the diffusion wave equation by simplifying state variables to model the impact of pressure gradients on flood dynamics. This method improved the equation's relevance to typical flow conditions [18]. In 2003, Caleffi et al. created a hydrodynamic model to simulate flooding along the Tossese River in Italy, examining the process of

 doi:10.20944/preprints202603.0241.v1

flood evolution [19]. In 2011, Zolghadr et al. utilised MIKE21 to model dam breaches, contrasting the findings with experimental data [20]. In 2023, Taylan E. Dilek developed a two-dimensional hydrodynamic model to identify flood risk zones in the Kinikli River basin. Flood water levels were measured at four key locations: the junction of the main，tributary streams of the River，main channel of the River and the outlet of the basin, to identify risk zones [21]. In 2025， Matej Vojtek et al. compared 1D and 2D hydraulic approaches for fluvial flood modeling of three flood scenarios (Q1000, Q100, Q10) using the MIKE + model and geographic information systems (GIS). and pointed out 1D model is not suitable for producing fluvial flood inundation maps in complex floodplains settings and 2D approach should be used instead for practical purposes[22].

In other sections or tributaries of Fuchun River, a segment of Qiantang River, examined in this study, researchers have performed a comprehensive hydrodynamic investigation, confirming the validity and dependability of hydrodynamic modelling for this waterway. Zhiping Sun et al. [23] utilised the MIKE21 hydrodynamic model to examine the water level variation characteristics of cross-river constructions, contrasting model simulations with empirical formula computations. Hangwei Zhu et al. [24] simulated the alterations in water impoundment and velocity prior to and following the optimisation of the levee line in the Jiuxi portion of the Qiantang River, examining the effects of levee modifications on flood control and tidal defence capabilities. Huoqi Yang et al. [25] developed a physical model of the Jiuxi riverbank section to evaluate the efficacy of water impoundment and overtopping volumes under two scenarios: the construction of the Changshun Dam and the elevation of the levee. Wenlong Cheng et al. [26] examined the propagation outcomes and differences between the tidal bore propagation simulated by two-dimensional and three-dimensional models of the Qiantang River. Yu Qiu et al. revealed formation mechanisms of three typical Qiantang tidal bores (cross-shape bore, thread-shape bore, and returned bore) ,and highlights how variations in flow discharge affect the tidal bore[27].

This study seeks to examine the hydrological effects on the river channel resulting from the modification of the former levee at Xinsha Island in Hangzhou using hydrodynamic modelling. Although in the study region, substantial research has been conducted on structures within the waterway, no comprehensive assessment has been undertaken on how modifications to the island's levee axis influence flood behavior.

A two-dimensional hydrodynamic river flow model is constructed adopting MIKE software and validated using existing observed data. Steady flow cases are performed for this river segment using four flood return periods: 10-year, 20-year, 50-year, and 100-year floods. A typical flood hydrograph is chosen, and a 20-year flood hydrograph is generated to perform in unsteady flow case.

2. Materials and Methods

2.1. Study Area and Purpose

Xinsha Island, located in Hangzhou City's Fuyang District, is a natural island in the Fuchun River. The island, located approximately 1 kilometre from Fuyang's major urban zone, is about 4.12 square kilometres. Its location is important along the Fuchun River's principal channel, dividing it into two navigable branches, one to the north and one to the south (Figure 1(a)). The region has a subtropical monsoon humid climate characterised by strong monsoon circulation, distinct seasons, abundant sunshine, and heavy precipitation concentrated in specific periods and locations. Typhoons frequently affect the region, resulting in significant yearly runoff. Typhoons often happen at the same time as the flood season, which makes flash floods and other secondary disasters more likely. The average elevation of the riverbed surrounding the island is -5 m, and its proximity to Qiantang Bay, combined with insufficient levee construction, results in floods happening less than once every three years. Currently, the majority of agricultural land on Xinsha Island lacks proper levee protection. The former levee cannot withstand prolonged periods of elevated water levels; hence it fails to meet flood defence and planning standards. The former levee currently covers less than 30% of the island's total land area. This study uses MIKE [28–30] software to construct a two-dimensional hydrodynamic river

 doi:10.20944/preprints202603.0241.v1

model that objectively examines the effect of variation of levee axis position on river flood flow at Xinsha Island and demonstrates its effectiveness.

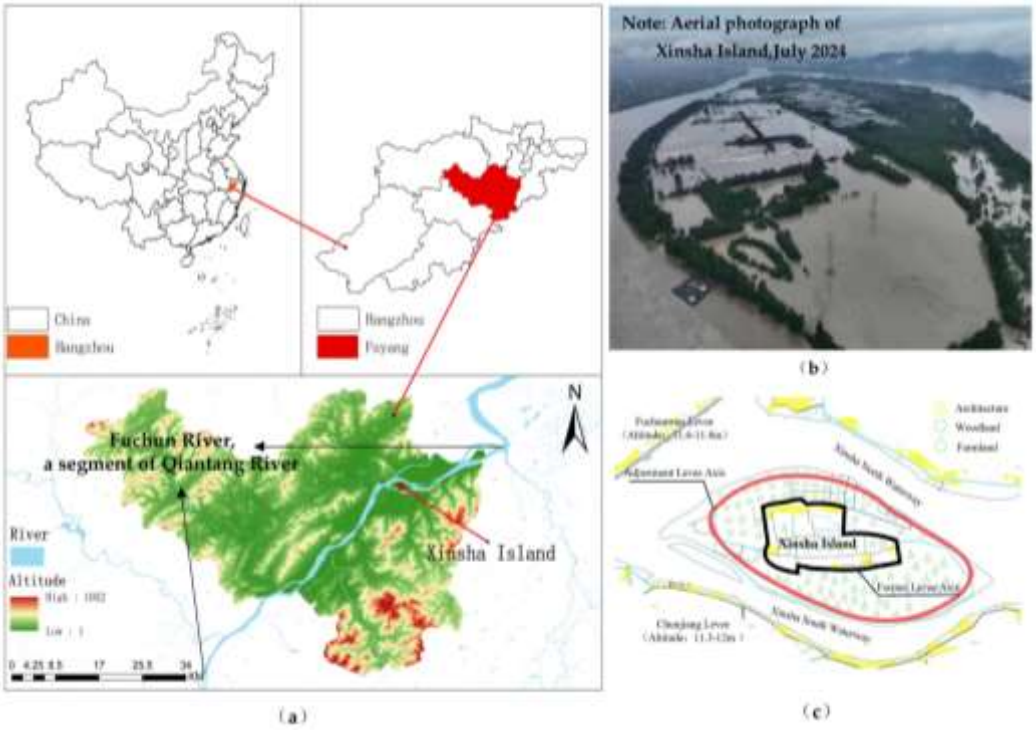

Figure 1. Xinsha Island location and status: (**a**)Where it is located; (**b**) Flood status of Xinsha Island; (**c**) Axis of Levee Position in Xinsha Island.

Given that Fuyang's urban area and the main river channel are located north of Xinsha Island, the levee axis has been primarily shifted to the southern side of the island to retain the northern waterway's flood discharge capacity whenever possible [31]. The previous Xinsha levee axis was approximately 4.67 kilometres long, surrounding a protected area of around 0.95 square kilometres. The levee, once modified, will reach 7.87 kilometres, safeguarding both southern agricultural land and northern floodplains. The modified perimeter now protects approximately 3.32 square kilometres, an increase of about 2.37 square kilometres. Figure 1(c) shows the revised levee axis. A steady flow model is constructed, taking into account design floods with return periods of 10, 20, 50, and 100 years. These four return periods offer a thorough representation of the effects of engineering adjustments on nearby water bodies during static conditions, which include both small-to-medium and large-scale flood events. An example flood hydrograph is used to establish the unsteady flow model. Using the prevalent design flood standard of a 20-year recurrence interval as an example, the unsteady flow model more effectively reflects the influence of engineering adjustments on nearby water bodies under varying flow conditions, thereby providing a more precise simulation of actual flood processes. The impact of a reduced flood discharge area caused by levee alterations on river flooding, using ten computational examples (Table 1) is investigated through the simulation, which includes three perspectives: water level variations, flow velocity variations and flow diversion ratio.

Table 1. Computational case.

Computational Case	Levee Status and Return Period
1	Former levee (10-year flood)
2	Adjustment levee (10-year flood)
3	Former levee (20-year flood)
4	Adjustment levee (20-year flood)

 doi:10.20944/preprints202603.0241.v1

5	Former levee (50-year flood)
6	Adjustment levee (50-year flood)
7	Former levee (100-year flood)
8	Adjustment levee (100-year flood)
9	Former levee (unsteady flow)
10	Adjusted levee (unsteady flow)

2.2. Two-Dimensional River Flow Modelling

2.2.1. Governing Equations

The primary governing equations for the model presented in this study are the two-dimensional unsteady shallow water equations, which are solved utilising the finite volume approach [22]. The continuity and momentum equations of the governing equations are as follows.

$$\frac{\partial h}{\partial t}+\frac{\partial h\bar{u}}{\partial x}+\frac{\partial h\bar{v}}{\partial y}=hs \tag{1}$$

$$\begin{aligned}\frac{\partial h}{\partial t}+\frac{\partial h\bar{u}^2}{\partial x}+\frac{\partial h\bar{u}\bar{v}}{\partial y}=&f\bar{v}h-gh\frac{\partial \eta}{\partial x}-\frac{h}{\rho_0}\frac{\partial P_a}{\partial x}-\frac{gh^2}{2\rho_0}\frac{\partial \rho}{\partial x}+\frac{\tau_{sx}}{\rho_0}-\frac{\tau_{bx}}{\rho_0}\\&-\frac{1}{\rho_0}\left(\frac{\partial S_{xx}}{\partial x}+\frac{\partial S_{xy}}{\partial y}\right)+\frac{\partial}{\partial x}(hT_{xx})+\frac{\partial}{\partial y}\left(hT_{xy}\right)+hu_sS\end{aligned} \tag{2}$$

$$\begin{aligned}\frac{\partial h\bar{v}}{\partial t}+\frac{\partial h\bar{v}\bar{u}}{\partial x}+\frac{\partial h\bar{v}^2}{\partial y}=&f\bar{u}h-gh\frac{\partial \eta}{\partial y}-\frac{h\partial P_a}{\rho_0\partial y}-\frac{gh^2}{2\rho_0}\frac{\partial \rho}{\partial y}+\\&\frac{\tau_{sy}}{\rho_0}-\frac{\tau_{by}}{\rho_0}-\frac{1}{\rho_0}\left(\frac{\partial S_{yx}}{\partial x}+\frac{\partial S_{yy}}{\partial y}\right)+\frac{\partial}{2}\left(hT_{xy}\right)+\frac{\partial}{2}\left(hT_{yy}\right)+hv_sS\end{aligned} \tag{3}$$

$$h\bar{u}=\int_{-d}^{\eta}udz h\bar{v}=\int_{-d}^{\eta}vdz \tag{4}$$

In the equations, h is water depth; t is time; x and y are horizontal coordinates, z is vertical coordinate; x, y and z constitute the right-handed Cartesian coordinate system; u and v are the components of the flow velocity in the x, y direction; $\bar{u}$ and $\bar{v}$ constitute the flow velocity averaged along the water depth; S is the source and sink item; f is the Coriolis parameter; g is the acceleration of gravity; η is the height of the water surface relative to the undisturbed base, i.e., the water level; ρ_0 is the density of the reference water; P_a is the local barometric pressure; and ρ is the water density. τ_{sx}, τ_{sy}, τ_{bx}, and τ_{by} are the components of the water flow shear stress in the x, y direction at the water surface and riverbed boundary; S_{xx}, S_{xy}, S_{yx}, and S_{yy} are the radial stress components; T_{xx}, T_{xy}, T_{yx}, and T_{yy} are the horizontal viscous stresses; and u_s and v_s constitute the velocity of water flow in the source and sink term.

2.2.2. Topography

Flood defence levees around Xinsha Island and along the Fuchun River are shown in Figure 1(c), where the former levee on the island is marked by black solid line and the adjusted levee by red solid line. The computational model is constructed using 1:10,000 topographic survey data, with a computational domain length of approximately 31 km. To ensure simulation accuracy, the Fuchun, Chunjiangwan, and former levees of Xinsha Island are appropriately generalised based on the topographical features and levee conditions of the river segment, resulting in the study region's landscape in Figure 2. The computational domain is divided using unstructured meshing, with localised mesh refinement carried out around Xinsha Island.

 doi:10.20944/preprints202603.0241.v1

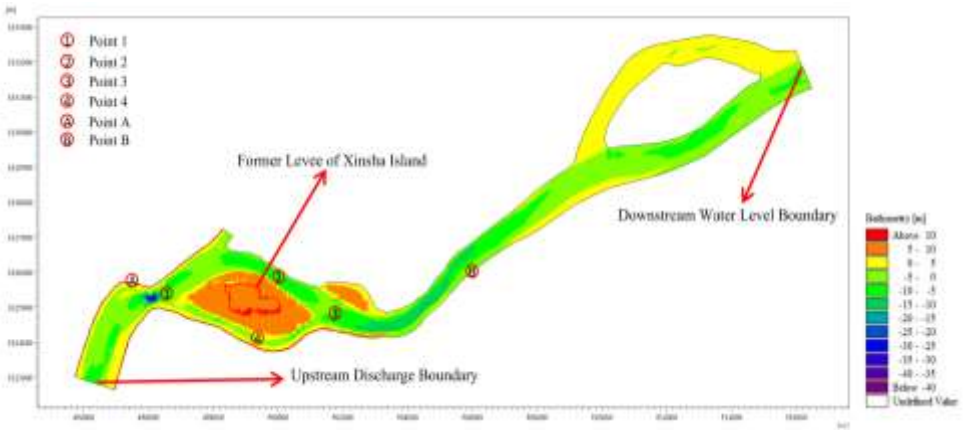

Figure 2. Schematic diagram of topography in the modelling area.

2.2.3. Boundary Conditions (BC)

2.2.3.1. Steady Flow Cases

(1) Upstream BC

Due to the convergence of many small and medium-sized rivers between the dam site of the Fuchun River Hydropower Station on the Qiantang River mainstem and the model's upstream boundary, the upstream boundary discharge must consider the impact of inter-basin influx. The inflow mostly derives from the Fuchun and Fenshui Rivers, the latter being controlled by the Fenshui River Hydropower Station. Feasibility studies and pertinent paperwork for other projects in the Qiantang River watershed indicate a significant probability of flood process superposition among the Fuchun River, Fenshui River, and Luzhu River. Nevertheless, due to artificial regulation, the probability of flood crests coinciding is minimal. Therefore, the flood discharge from the Fenshui River and its tributaries necessitates the evaluation of their respective coordinated management scenarios. The inflow at the upstream boundary, specifically the Fuyang Station flow, consists of two elements: the primary flood from the discharge of the Fuchun River Hydropower Station and the residual flow from the confluence of floods in the Fenshui River, Luzhu River, and other associated watercourses. By calculating the difference in peak discharge between the Fuchun River Hydropower Station and the downstream Wenjiayan Hydrological Station throughout various return periods, the cumulative input from each tributary within the area is established. The discharge is subsequently distributed proportionally to the catchment area of each tributary, employing a constant flow methodology for confluence to ascertain the design flood peak discharge at the Fuyang Station on the upstream boundary (Table 2).

Table 2. Maximum design peak discharge.

Return Periods(year)	10	20	50	100
Tributary Inflow（m^3）	640	850	1085	1090
Fenshui River Inflow（m^3）	920	1150	1415	1610
Discharge from the Fuchun River Power Station（m^3）	15240	17300	21600	23100
Discharge at Fuyang Station — Upstream Boundary（m^3）	16800	19300	24100	25800

(2) Downstream BC

 doi:10.20944/preprints202603.0241.v1

The flood level in the Fuyang segment of the Fuchun River is influenced by both the maximum flood discharge and the water level effect of tidal currents in the downstream estuary portion. Due to the closeness of the downstream simulated boundary to the Wenjiayan hydrological station, the design flood level at the lower boundary in this model utilises the design flood level from the Wenjiayan hydrological station (Table 3).

Table 3. Design flood stage at Wenjiayan hydrological station.

Return Periods(year)	10	20	50	100
Flood level（m）	7.84	8.4	9	9.3

2.2.3.2. Unsteady Flow Cases

Unsteady flow modelling, unlike its steady flow counterpart, primarily focuses on the full dynamics of temporal flow variations, thus providing a more precise representation of the effects of structural alterations on surrounding water bodies during periods of rapid flow change. As a result, the return period of a 20-year flood event is used with recorded water level and discharge data. A transient flow model is then constructed for this situation to simulate and compare the time-dependant hydrodynamics both before and after the engineering intervention, at various time intervals.

In the absence of recorded flood progression data, a univariate analysis is performed, comparing water level to discharge by combining available discharge and water level observations. The results are shown in Figure 3. The graph has an R-squared value of 0.9118, indicating a strong relationship between water level and discharge. Representative floods are chosen as typical hydrographs by analysing the completeness of the observed flood data, the season of occurrence, the shape of the peak, the location of the main peak, and the duration of the flood. The July 2024 flood, primarily caused by heavy rain during the plum rain season, showed a high level of data completeness, a clear peak, and the largest discharge, making it a good example. Therefore, the July 2024 flood is used as a representative flood hydrograph. The flood process's 20-year return period is determined by analysing the water level and discharge data.

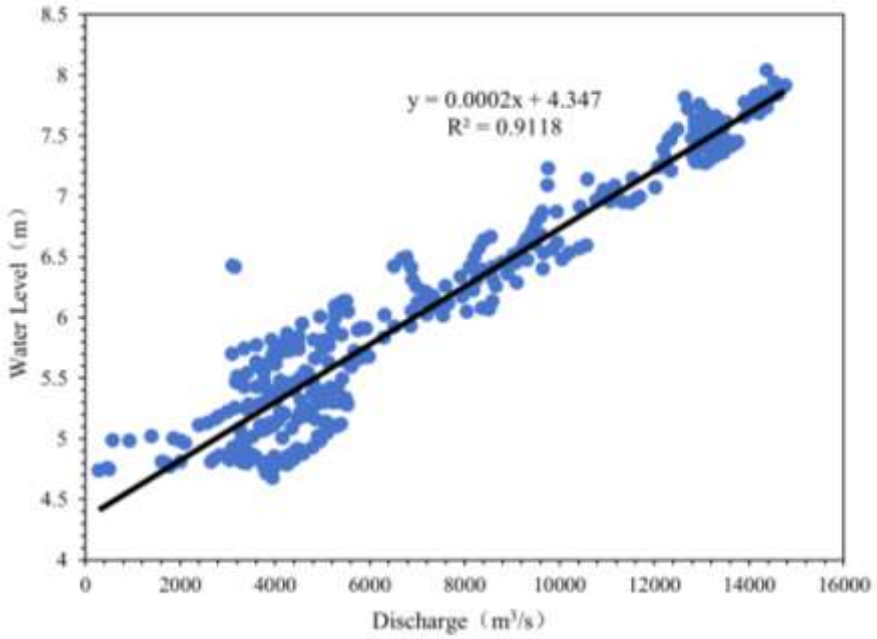

Figure 3. Relationship between water level and discharge.

 doi:10.20944/preprints202603.0241.v1

(1) Upstream Unsteady Flow

The upstream boundary is defined by a discharge boundary. The Fuyang Station experienced a peak flow of 19,300 m^3/s during the 20-year return period flood. Interestingly, the most significant flood flow recorded, which occurred in July 2024, reached 14,756 m^3/s. The flow values in the standard flood hydrograph are adjusted based on the ratio of the 20-year design flood's peak discharge to the highest discharge that is actually observed. This scaling method ensures that the increased peak discharge matches the 20-year flood peak observed at Fuyang Station, which then allows for the creation of the 20-year flood hydrograph.

(2) Downstream Unsteady Flow

Using the amplified discharge process curve in the equation derived from the single-value analysis of the relationship between water level and discharge (Figure 3), we can create the water level process curve for a 20-year flood event. Figure 4 shows the process curve, which illustrates the changes in water level and discharge over time during the 20-year flood.

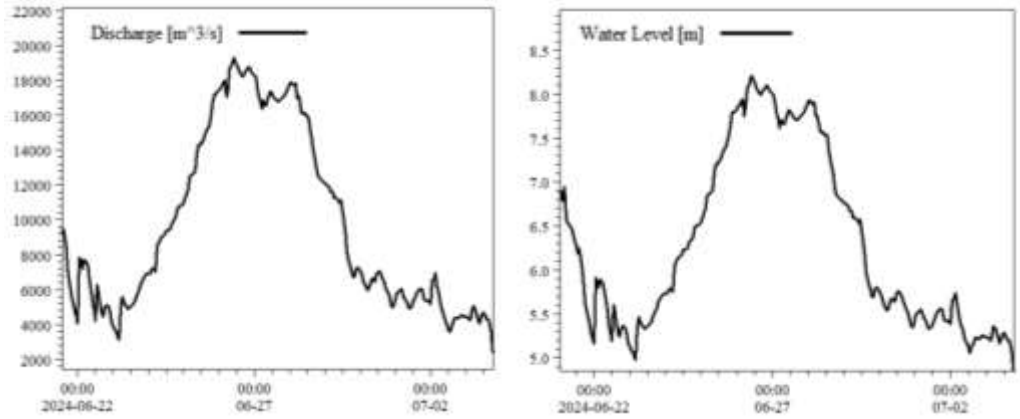

Figure 4. Water level and discharge for the 20-year return period event.

2.2.4. Calibration and Validation

2.2.4.1. Measured Discharge and Water Level Data

The unsteady flow model is used to calibrate and validate the parameters of the Fuchun River model for the Fuyang section. The June 2020 flood event served as the BC for model calibration, while the July 2024 flood event provided the BC for model validation. Figure 5 shows the related water level and discharge changes. Figure 3 shows that during calibration, the maximum upstream discharge boundary was 13681 m^3/s, whereas the maximum downstream water level boundary was 7.52m. During validation, the upstream discharge boundary reached 14756 m^3/s, while the downstream water level boundary peaked at 8.02 m. Changes in upstream discharge have a significant impact on water levels in the Fuchun River, with a generally steady tendency.

 doi:10.20944/preprints202603.0241.v1

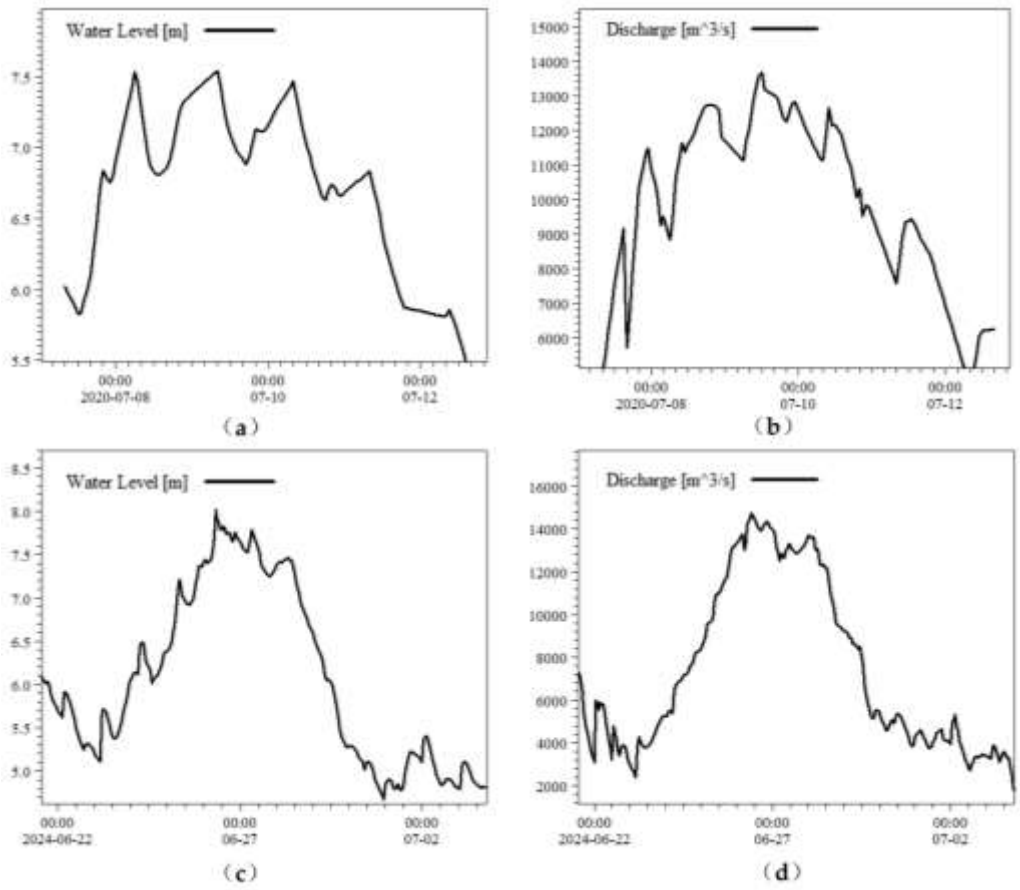

Figure 5. Measured water level and discharge: (**a**)Water level BC for validation; (**b**) Discharge BC for validation; (**c**) Water level BC for calibration; (**d**) Discharge BC for calibration.

2.2.4.2. Mesh Sensitivity

Three meshes of varied density and mass are created using comparable settings, such as roughness coefficient and BC (Table 4). Using flood process data from July 2024 as BC, changes in water level and flow velocity are examined at four locations around the island, Points 1, 2, 3, and 4 (refer to Figure 2) to assess the justification for mesh design (Figure 6). The results show that simulated water levels are largely constant over multiple grids, with a maximum absolute inaccuracy of 0.05m. Mesh 2 produces more consistent flow velocity simulations than Mesh 1. Mesh 3 shows a small increase in flow velocity over Mesh 1, with a maximum absolute error of 0.03 m/s, which is within acceptable limits[32]. Therefore, Mesh 1 was selected for additional simulation studies.

Table 4. Mesh density.

Mesh Case	Mesh Count	Minimum Mesh Size(m^2)
Mesh 1	89596	37
Mesh 2	100958	24
Mesh 3	191754	19

 doi:10.20944/preprints202603.0241.v1

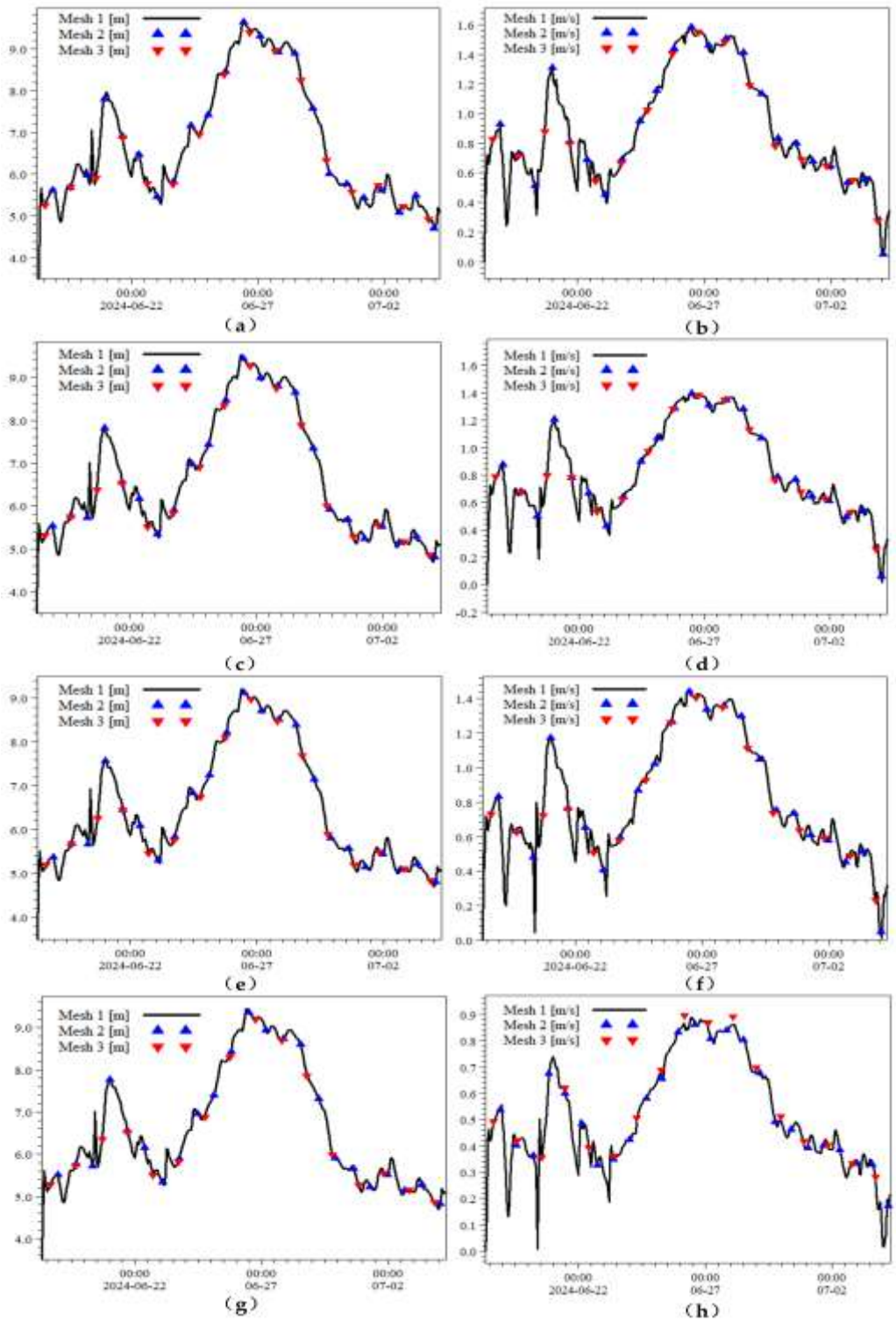

Figure 6. Mesh sensitivity and comparison: (**a**)Point 1 water level; (**b**) Point 1 velocity; (**c**) Point 2 water level; (**d**) Point 2 velocity; (**e**) Point 3 water level; (**f**) Point 3 velocity; (**g**) Point 4 water level; (**h**) Point 4 velocity.

2.2.4.3. Calibration and Validation Result

Initial roughness parameters for the model are presented in Table 5 [33,34], and a calibration and validation analysis is conducted using historical flood data. Flood events for the Fuyang segment of the Fuchun River in June 2020 and July 2024 are simulated to calibrate and validate parameters. The upstream boundary uses flood discharge data, whereas the downstream boundary employs recorded flood water levels. The time-series profiles are generated, depicting fluctuations in water level and discharge as illustrated in Figure 5. Calibration and validation points are designated as Points A and

 doi:10.20944/preprints202603.0241.v1

B in Figure 2, with results depicted in Figure 7. The calibration and validation results indicate that the maximum absolute error in calibrated water levels is 0.1 m, while the highest absolute error in validated water levels is 0.31 m. Simulated results demonstrate significant agreement with the measured values, accurately reflecting the flow dynamics of the Fuchun River.

Table 5. Initial roughness parameters.

Area	Roughness
waterway	0.025–0.04
Floodplain	0.06–0.08
Residential facilities	0.06–0.08
Grassland	0.025–0.04
Woodland	0.05–0.08
Farmland	0.035–0.05
Bare land	0.035–0.05

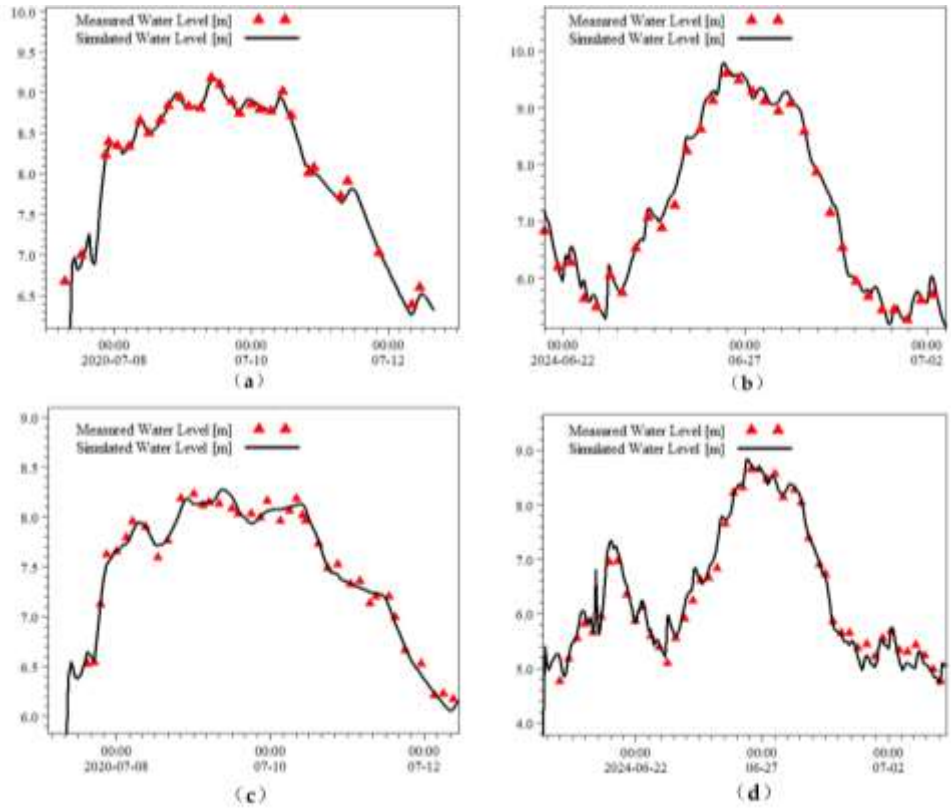

Figure 7. Water level calibration and validation: (**a**)Point A calibration; (**b**) Point A validation; (**c**) Point B calibration; (**d**) Point B calibration.

3. Results

3.1. Steady Flow

3.1.1. Water Level Variations

The water level difference on both sides of the levee is driven by the combined effects of riverbed topography, the island levee axis, the roughness coefficient, and other factors. The simulation results comprehensively account for these multiple influences. According to the model's calculated water levels, following the adjustment of Xinsha Island's levee axis, the water level difference values range for a 10-year flood event is from -0.037 to 0.099 m; for a 20-year flood event, from -0.048 to 0.102 m; for a 50-year flood event, from -0.107 to 0.162 m; and for a 100-year flood, from -0.128 to 0.183 m. The

 doi:10.20944/preprints202603.0241.v1

levee adjustment causes water level increasing in the southern waterway and water level decreasing in the northern waterway. Comparing the water level difference on both sides of the levee for 10-year, 20-year, 50-year, and 100-year flood return periods reveals that as the flood return period increases, the magnitude of water level difference changes on both sides of the river also increases, with the changes gradually stabilising. The water level difference conditions for different flood frequencies are shown in Figure 8.

Figure 8 shows that the water level around the island varies from -1.5% to 2%, compared that after adjustment of the levee to the former one. In the adjustment levee, water level at the upstream of the island rises to a certain degree, the water level in the middle of the northern waterway and downstream of the island decreases, the reason is that the adjusted levee encloses permanent farmland and floodplains on the island's northern and southern flanks. River water levels exhibit high sensitivity to discharge variations. As discharge increases, amplitudes of the water level rise and fall on both northern and southern waterway are enlarged, most notably in the central sections of the northern and southern waterway and at the downstream of island.

After adjustment of the island levees, both riverbanks of the Fuchun River generally have sufficient capacity to withstand flood surges during 10-year, 20-year, 50-year, and 100-year flood return periods. Water level in the Xinsha South waterway and the upstream of the island will relatively modest rise up. Overall, the levee adjustment exerts a negligible impact on river water levels while effectively alleviating flood threat on the northern waterway and downstream sections of the island's watercourse.

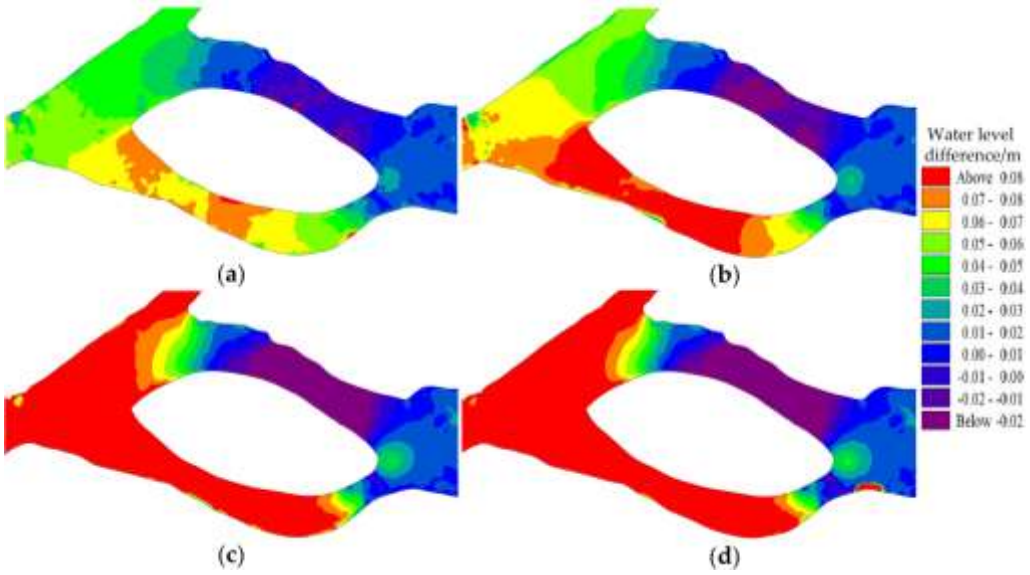

Figure 8. Water level difference between adjustment and former levee (steady flow): (**a**) 10-year flood; (**b**) 20-year flood; (**c**) 50-year flood; (**d**) 100-year flood.

3.1.2. Flow Velocity Variations

The flow velocity variation for the 10-year flood event along the adjusted levee axis of Xinsha Island ranges from -0.859 to 0.473 m/s; for the 20-year flood event, it ranges from -1.174 to 0.652 m/s; for the 50-year flood event, it ranges from -0.698 to 1.252 m/s; and for the 100-year flood event, flow velocities range from -0.508 to 0.785 m/s. Comparing the flow velocity variation values after the adjustment of levee to the farmer one, the patterns of flow velocity increase or decrease are largely consistent across four different return periods. The flow velocity variations for different flood frequencies are illustrated in Figure 9.

Figure 9 shows that due to the levee adjustment, the obstruction effect on the southern waterway is pronounced. Under all return periods, both northern and southern waterway velocities exhibit a

 doi:10.20944/preprints202603.0241.v1

pattern where southern flow slows while northern flow accelerates, consistent with water level variations. For all four return periods cases, flow velocity variations generally remain within ±0.3 m/s. From middle segment to downstream of the Xinsha South waterway, flow velocity abruptly changes due to the influence of the width of the waterway shortening. The adjustment levee axis substantially narrows the waterway width while adopting a smoother profile, concentrating flow within the main channel. This modification increases velocities, lowers water levels, and achieves significant diversion effects. In the adjustment levee, the Xinsha north waterway exhibits markedly increased flow velocities in the middle of the waterway during four return periods, while near levee velocity variation is negligible. Conversely, flow velocities in the upstream of the Xinsha South waterway slow down, while that in the downstream speed up.

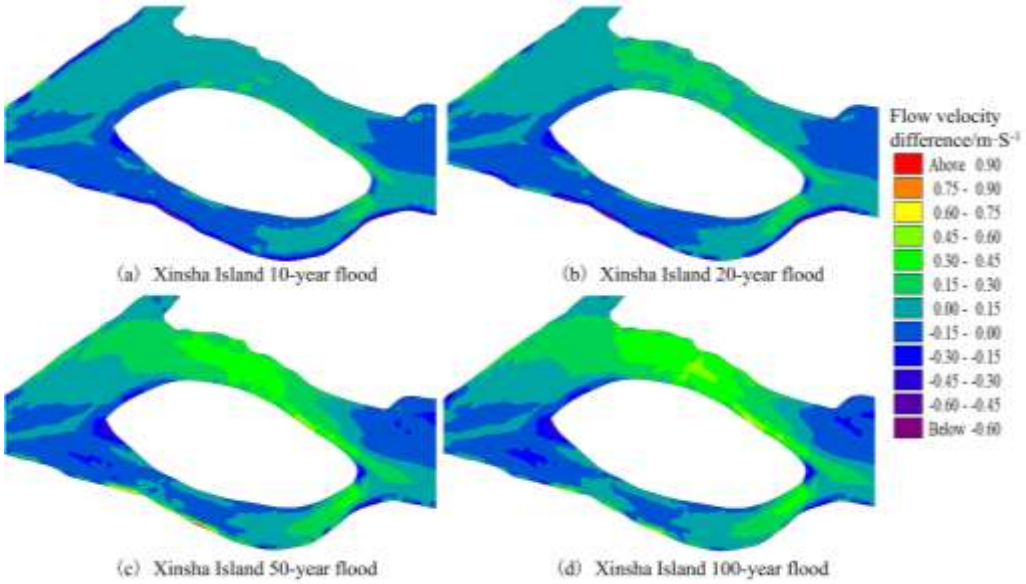

Figure 9. Flow velocity difference between adjustment and former levee (steady flow): (**a**) 10-year flood; (**b**) 20-year flood; (**c**) 50-year flood; (**d**) 100-year flood.

3.1.3. Flow Division Ratio Variations

The flow diversion ratio is a crucial parameter for bifurcated river sections, representing the ratio of discharge through a particular branch channel to the total river discharge. Variations in the flow diversion ratio directly influence on flood control, navigation, water intake, and drainage; they play a significant role in the conservation and utilisation of bifurcated river sections either. The flow diversion ratio for the northern and southern waterways after the adjustment and the former levee is listed in Table 6 during four flood return periods. The flow diversion ratios for the northern and southern waterways remain largely stable around 1:3 before and after the adjustment of levee axis. Moreover, regardless of flood frequency variations, the flow diversion ratios are basically consistent. As upstream discharge increased or the flood return period longer, the flow diversion ratio slightly decreases in the northern main channel, which slightly increases in the southern waterway. In the status of the former levee, from the flood return period of 10 years to 100 years, the flow diversion ratio decrease from 75.5% to 72.5% in the northern waterway, while the flow diversion ratio rise from 24.5% to 27.5% in the southern waterway, which indicates that under the former levee status, the diversion effect of the southern waterway intensified with larger flood discharge. In the case of the adjustment levee, the flow diversion ratio at each return period is slightly higher in the northern waterway, while the overall decreasing trend of the flow diversion ratio in the northern waterway is the same as that in the former levee status. The flow diversion ratio situation is exactly the opposite in the south waterway. In addition, it is demonstrated that the engineering measures of adjustment of the levee have effectively enhanced and stabilised the northern waterway's discharge capacity

 doi:10.20944/preprints202603.0241.v1

during heavy flooding. The magnitude of change in flow diversion ratio increases with longer flood return periods. That is, the change's value is from 2.0% at the 10 years return period to 2.9% at the 100 years return period. It is shown that levee adjustment yields more pronounced regulatory effects during heavy flooding.

Table 6. Flow division ratio in steady flow.

Return Periods	Levee Status	North Waterway	South Waterway
10-year flood	Former levee	75.5%	24.5%
	Adjustment levee	77.5%	22.5%
20-year flood	Former levee	74.5%	25.5%
	Adjustment levee	76.8%	23.2%
50-year flood	Former levee	73.0%	27.0%
	Adjustment levee	75.8%	24.2%
100-year flood	Former levee	72.5%	27.5%
	Adjustment levee	75.4%	24.6%

3.2. Unsteady Flow

Compared to steady flow modelling, unsteady flow modelling not only reveals spatial variations of flood characteristics but also describes temporal flood processes. To assess flood evolution patterns, temporal and spatial analysis is conducted for water level variations, flow velocity variations and flow division ratio.

3.2.1. Water Level Variations

In temporal analysis, the flooding water level time histories at four points are discussed, the locations of points 1, 2, 3, and 4 as shown in Figure 2, are presented in Figure 10, which includes that in the former levee status and the adjustment levee status. The unsteady flow flooding simulation describes the flood occurring from 25th June 2024 to 1st July 2024. In spatial analysis, four temporal snapshots are selected to analyse water accumulation patterns in the Xinsha Island area at different moments, as depicted in Figure 11. The numbers shown in the figure represent the water level difference between the adjusted levee configuration and the original levee configuration.

Figure 10 shows that the flood peak time, rise and fall process are largely consistent. In the adjusted levee condition, peak time water levels at points 1 and 3 are marginally higher than that in the former condition, with the maximum rise reaching 0.071 m. Conversely, peak time water levels at points 2 and 4 are marginally lower with the maximum fall reaching -0.009 m.

Figure 11 shows that in the adjusted levee condition, water level rises in the southern waterway and falls in the northern waterway, which benefits flood discharge in the northern waterway. When upstream discharge increases, water level rise and reduction in both the southern and northern waterways intensify. When upstream discharge decreases, the water level rises and the reduction in both the southern and northern waterways alleviates. The primary location of water level variation occurs in the middle of waterways. The maximum water level difference reaches 0.124 m, while the maximum reduction is -0.048 m.

 doi:10.20944/preprints202603.0241.v1

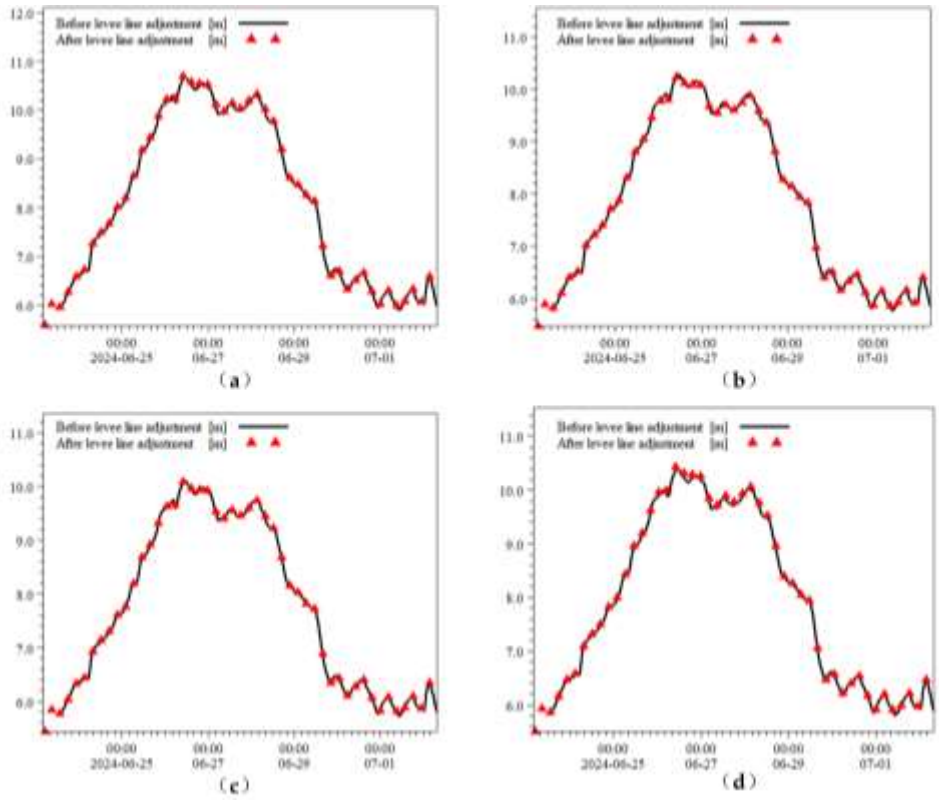

Figure 10. Comparison of water level :(**a**) Point 1; (**b**) Point 2; (**c**) Point 3; (**d**) Point 4.

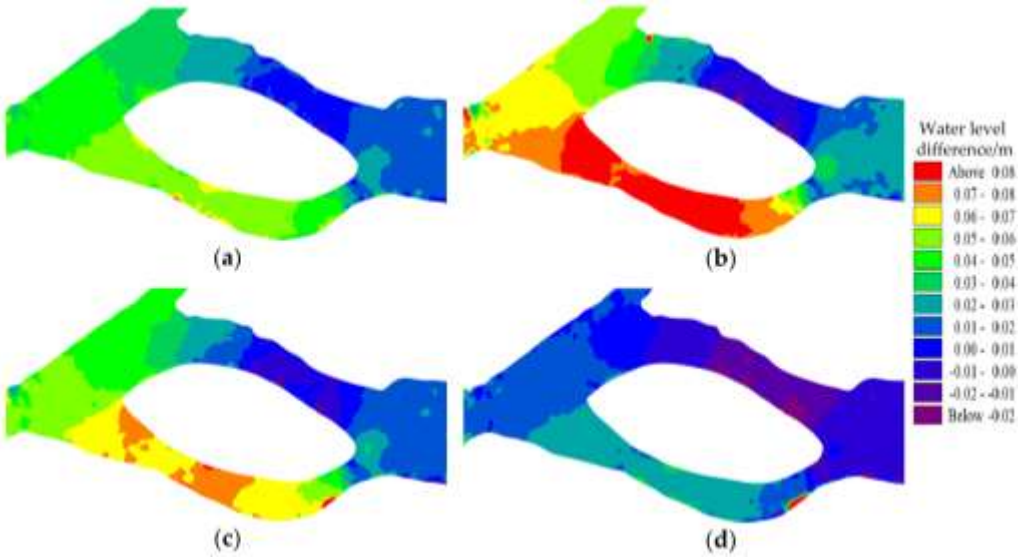

Figure 11. Water level difference between adjustment and former levee(unsteady flow) :(**a**) At 15:00 25th June, upstream discharge 14258 m³/s; (**b**) At 10:00 26th June, with an upstream boundary discharge of 19300 m³/s; (**c**) At 11:00 27th June, with an upstream boundary discharge of 17393 m³/s; (**d**) At 16:00 28th June, with an upstream boundary discharge of 14086 m³/s.

3.2.2. Flow Velocity Variations

The impact of levee adjustment on the river channel manifests as a dual response in water level and flow velocity, essentially representing a temporal and spatial reorganisation of the channel's hydraulic characteristics. Therefore, a comprehensive comparative analysis of flow velocity changes is conducted across both temporal and spatial dimensions. Temporally, the time histories of flow velocity at four points are presented in Figure 12, and the locations of these points are shown in Figure

 doi:10.20944/preprints202603.0241.v1

2. These flow velocity time histories are compared between the adjusted levee condition and the original levee condition. Spatially flow velocity differences between the adjusted levee condition and the original levee condition are depicted in Figure 13, where four temporal snapshots are selected, each snapshot with the same time in the adjustment levee status and the former levee status.

Figure 12 shows that the trends of flow velocity increase and decrease before and after levee axis adjustments at the four points are broadly consistent, while the magnitude of variation is more pronounced. At peak times, flow velocities at points 1 and 3 in the adjusted levee status are marginally lower than that in the former levee status, the maximum difference is -0.045 m/s. Conversely, flow velocities at points 2 and 4 in the adjusted levee status are marginally higher than that in the former levee status, the maximum difference is 0.101 m/s.

Figure 13 shows that in the adjusted levee status, flow velocity increases in the northern waterway and decreases in the southern waterway. When upstream discharge increases, the velocity difference in the northern waterway increases while that in the southern waterway decreases, as depicted in Figures 13(a) and (b). Conversely, as illustrated in Figures 13(b) and (c), the velocity difference in the southern waterway increases while it decreases in the northern waterway when upstream discharge decreases.

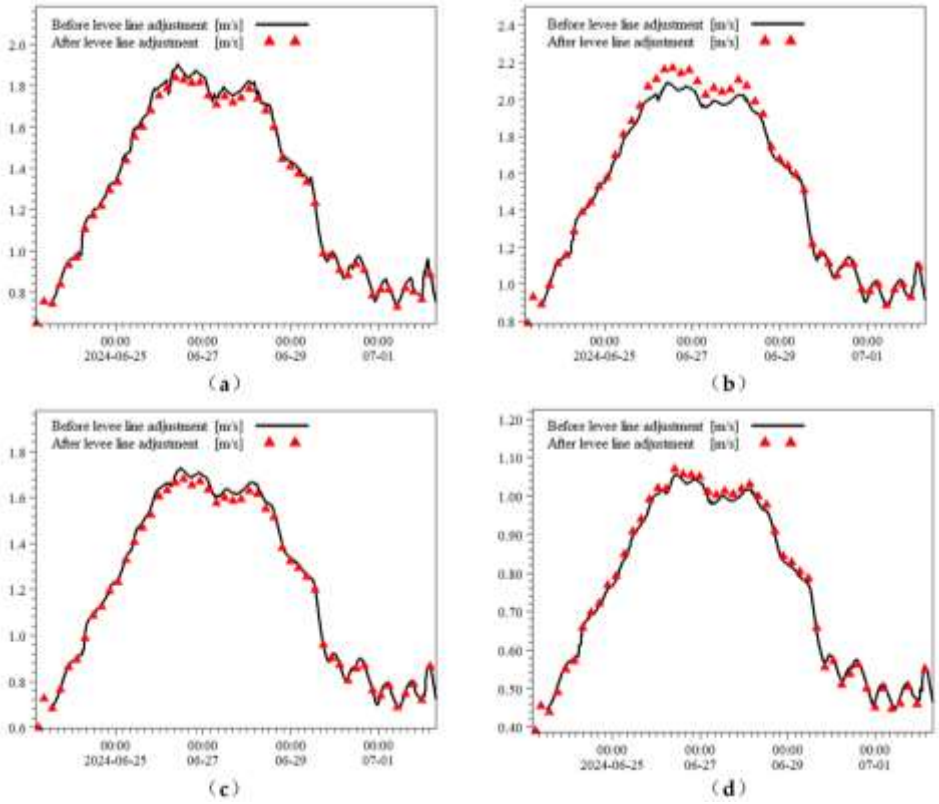

Figure 12. Comparison of Flow Velocity:(**a**) Point 1; (**b**) Point 2; (**c**) Point 3; (**d**) Point 4.

 doi:10.20944/preprints202603.0241.v1

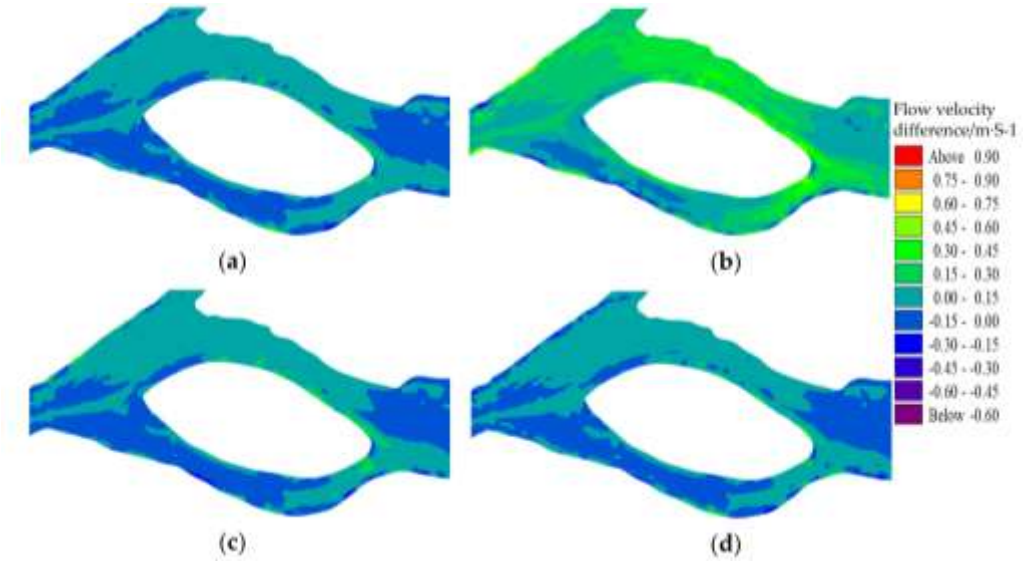

Figure 13. Flow velocity difference between adjustment and former levee(unsteady flow):(**a**) At 15:00 25th June, upstream discharge 14258 m³/s; (**b**) At 10:00 26th June, with an upstream boundary discharge of 19300 m³/s; (**c**) At 11:00 27th June, with an upstream boundary discharge of 17393 m³/s; (**d**) At 16:00 28th June, with an upstream boundary discharge of 14086 m³/s.

3.2.3. Flow Division Ratio Variations

The diversion ratio fluctuates during the flood progression. Figure 14 illustrates the variations in discharge values for the northern and southern waterways before and after the levee modification, while Table 7 presents the flow diversion ratios at four different times. During periods of low upstream discharge, the discharge difference on each side of the river waterway remains rather stable in the adjustment levee status and that in the former levee status. When attaining a certain discharge value, the southern waterway demonstrates an increased discharge relative to the former levee, while the northern waterway experiences an equal decrease. The flow difference intensifies with increasing upstream flow, reaching a maximum of 350 m³/s at the flood peak. In the adjustment levee status, the diversion ratio of the northern waterway has increased, while that of the southern waterway has decreased.

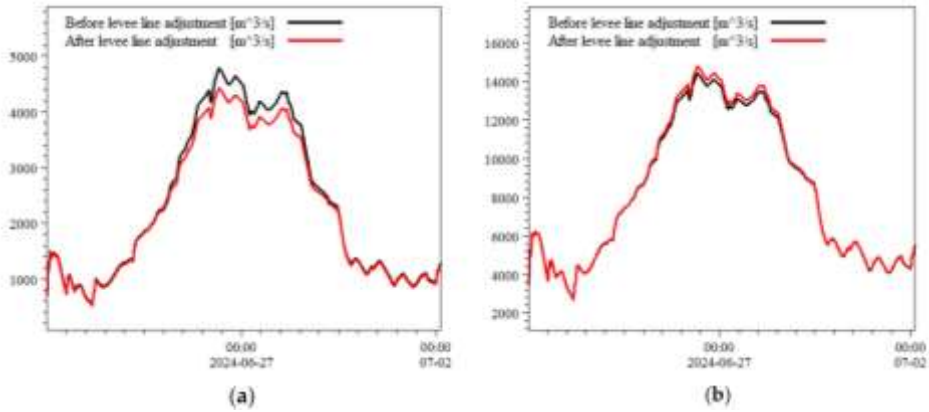

Figure 14. Discharge in unsteady flow (**a**) South waterway; (**b**) North waterway.

Table 7. Flow Division Ratio in unsteady Flow.

Time	Levee Status	North Waterway	South Waterway
2024/06/25/15:00	Former levee	77.1%	22.9%
	Adjustment levee	78.0%	22.0%

 doi:10.20944/preprints202603.0241.v1

2024/06/26/10:00	Former levee	75.1%	24.9%
	Adjustment levee	76.9%	23.1%
2024/06/27/11:00	Former levee	75.8%	24.2%
	Adjustment levee	77.2%	22.6%
2024/06/28/16:00	Former levee	78.2%	21.8%
	Adjustment levee	78.9%	21.1%

4. Discussion

The Xinsha Island levee constitutes a vital component of the Fuchun River flood control system. The levee axis adjustment will solve some existing issues, such as the incomplete closure of the flood protection, suboptimal flood defence capacity and river flow variation etc. A two-dimensional hydrodynamic model is adopted to systematically evaluate the variation of water level, flow velocity and flow division ratio resulting from the adjustment level compared to the former levee under steady and unsteady flow. It is indicated that the reduction of the river's floodplain area does not necessarily imply increasing flood risk.

A simple reduction in the floodplain area typically results in water level increase, yet the levee adjustment effect is comprehensive, which simultaneously alters floodplain area, flow velocity distribution, water level, boundary roughness, and flow division. The levee enlarges the island's protected area and induces upstream water level increasing, changes flow velocity in the southern and northern waterway, reduces lower flow area and eddies area. The adjusted levee surrounded area on the northern side of the island primarily comprises inland floodplain, which is characterised by dense vegetation with relatively high roughness. This zone contributes little to effective flow capacity while increasing wet perimeter and frictional resistance. After the levee adjustment, water level in the northern waterway descended, accompanied by a corresponding flow velocity speed up. The phenomenon demonstrates that flow is confined to a narrow efficient channel, with decreasing wet perimeter and increasing flow velocity, thereby causing the water level to drop. In the downstream area, there forms a slow-flow zone because of the confluence of the two channels, which could be seen from the water level and flow velocity difference figures. In this area, water flow kinetic energy is converted into potential energy, causing the water level rises slightly in the adjusted levee status compared to the former levee status. However, downstream far away from this area, the water level drops markedly in the adjustment levee status, falling below that in the former levee status. Overall, the simulation results demonstrate that adjusting the former levee axis at Xinsha Island effectively reduces flood threat on the levee protection, which provides reliable justification for the levee adjustment.

5. Conclusions

A two-dimensional hydrodynamic numerical model is adopted to simulate steady and unsteady flow flood processes in the Xinsha Island River segment due to its levee adjustment for flood protection, in which steady flow is conducted under four return periods 10-year, 20-year, 50-year and 100-year, and unsteady flow is studied under 20-year return period. Some conclusions are summarized as follows.

(1) Water level variation in southern and northern waterways basically consistent under steady and unsteady flow. There exists water level rising in the southern waterway, the longer the flood return period, the higher the water level. Water level descends occur in northern waterway, the longer the flood return period, the lower the water level. The water level rising occurs in the middle and downstream of the southern waterway, with a maximum rising value of 0.183 m. Water level descend is observed in the middle of the northern waterway, with a maximum descending value of -0.128 m.

(2) Under steady and unsteady flow, velocity variation is almost in agreement in both the southern and northern waterways. Flow velocity slows slightly in the southern waterway, at its upstream, the descending value is in the range of -0.15 m/s to -0.3 m/s. Flow velocity increases slightly

 doi:10.20944/preprints202603.0241.v1

in the northern waterway, in the middle of the waterway with values rising in the range of 0.15 m/s to 0.45 m/s. The flow diversion ratio between the southern and the northern waterway remains largely stable which approximately 1:3 under steady and unsteady flow. This adjustment levee scheme effectively enhances the diversion capacity of the northern waterway of Xinsha Island and slightly drops the flow diversion ratio in the southern waterway.

Author Contributions: Conceptualization, W.Y. and H.G.; methodology, H.G.; data curation, W.Y.; writing—original draft preparation, W.Y.; writing—review and editing, H.G., D.W., E.C.M. and J.Z.; project administration, H.G.; funding acquisition, H.G. and D.W. All authors have read and agreed to the published version of the manuscript.

Funding: This research was funded by Nation Natural Science Foundation of China, grant number 52401330.

Data Availability Statement: The raw data supporting the conclusions of this article will be made available by the authors on request.

Conflicts of Interest: The authors declare no conflict of interest.

References

1. Ding, W.; Wu, J.; Tang, R.; Chen, X.; Xu, Y. A Review of Flood Risk in China during 1950–2019: Urbanization, Socioeconomic Impact Trends and Flood Risk Management. *Water* **2022**, *14*, 3246, doi:10.3390/w14203246.
2. Zhang, K.; Ji, Z.; Luo, X.; Liu, Z.; Zhong, H. Flood Simulation in the Complex River Basin Affected by Hydraulic Structures Using a Coupled Hydrological and Hydrodynamic Model. *Water* **2024**, *16*, 2383, doi:10.3390/w16172383.
3. Harvey, G.L.; Thorne, C.R.; Cheng, X.; Evans, E.P.; J.D. Simm, S.H.; Wang, Y. Qualitative Analysis of Future Flood Risk in the Taihu Basin, China. *J Flood Risk Management* **2009**, *2*, 85–100, doi:10.1111/j.1753-318X.2009.01024.x.
4. Gao, Y.; Li, F.; Mao, L.; Yan, N.; Peng, C.; Tao, H.; Zhang, D. Simulation on Water Quality of Reservoir at Construction Phase by Pollutant Release from Oxidation of Waste Rocks Rich S and Fe. *Environmental Technology & Innovation* **2022**, *28*, 102860, doi:10.1016/j.eti.2022.102860.
5. Hu, K.; Zhang, W.; Wang, X. Simulation of the Impact of Breakwaters on Hydrodynamic Environment in Laizhou Bay, China. *J. Ocean Univ. China* **2022**, *21*, 1557–1564, doi:10.1007/s11802-022-5278-6.
6. Jiang, S.H.; Zhi, H.L.; Wang, Z.Z.; Zhang, S. Enhancing Flood Risk Assessment and Mitigation through Numerical Modeling: A Case Study. *Nat. Hazards Rev.* **2023**, *24*, 04022046, doi:10.1061/NHREFO.NHENG-1687.
7. Zhang, X.; Wang, T.; Duan, B. Study on the Effect of Morphological Changes of Bridge Piers on Water Movement Properties. *Water Practice and Technology* **2021**, *16*, 1421–1433, doi:10.2166/wpt.2021.080.
8. Quan, C.; Wang, D.; Li, X.; Yao, Z.; Guo, P.; Jiang, C.; Xing, H.; Ren, J.; Tong, F.; Wang, Y. Waterway Regulation Effects on River Hydrodynamics and Hydrological Regimes: A Numerical Investigation. *Water* **2025**, *17*, 1261, doi:10.3390/w17091261.
9. Sabeeh, N.N.; Alabdraba, W.M.Sh. The Hydrodynamic Model Using HEC-RAS: The Case of Tigris River Downstream of Samarra Barrage (Iraq). *IOP Conf. Ser.: Earth Environ. Sci.* **2022**, *1120*, 012017, doi:10.1088/1755-1315/1120/1/012017.
10. Alhumoud, J. ANALYSIS AND EVALUATION OF FLOOD ROUTing USing MUSKINGUM METHOD. *J Appl Eng Science* **2022**, *20*, 1366–1377, doi:10.5937/jaes0-37455.
11. Shan, C.; Guo, H.; Dong, Z.; Liu, L.; Lu, D.; Hu, J.; Feng, Y. Study on the River Habitat Quality in Luanhe Based on the Eco-Hydrodynamic Model. *Ecological Indicators* **2022**, *142*, 109262, doi:10.1016/j.ecolind.2022.109262.
12. Yi, Y.; Tang, C.; Yang, Z.; Zhang, S.; Zhang, C. A One-Dimensional Hydrodynamic and Water Quality Model for a Water Transfer Project with Multihydraulic Structures. *Mathematical Problems in Engineering* **2017**, *2017*, 2656191, doi:10.1155/2017/2656191.

 doi:10.20944/preprints202603.0241.v1

13. Han, S.; Yu, X.; Zhang, W.; Sang, G.; Liu, Y.; Xu, S. Rationality Research on Pumping Station Location Based on MIKE Model: A Case Study of the Wanfu River Re-Navigation Project. *Water* **2023**, *15*, 4207, doi:10.3390/w15244207.
14. Gao, H.; Hu, J.; Zhao, H.; He, D.; Zhang, S.; Shi, D.; Li, P.; Zhang, Z.; Cui, J. Evaluating the Impact of Bridge Construction on Flood Control Capacity in the Eastern Coastal Regions of China Based on Hydrodynamic Modeling. *Water* **2025**, *17*, 1675, doi:10.3390/w17111675.
15. Ye, C.; Xu, Z.; Lei, X.; Zhang, R.; Chu, Q.; Li, P.; Ban, C. Assessment of the Impact of Urban Water System Scheduling on Urban Flooding by Using Coupled Hydrological and Hydrodynamic Model in Fuzhou City, China. *Journal of Environmental Management* **2022**, *321*, 115935, doi:10.1016/j.jenvman.2022.115935.
16. Isaacson, E.; Stoker, J.J.; Troesch, A. Numerical Solution of Flow Problems in Rivers. *J. Hydr. Div.* **1958**, *84*, 1–18, doi:10.1061/JYCEAJ.0000220.
17. Cunge, J.A. Discussion of "Computer Simulation of Unsteady Flows in Waterways." *J. Hydr. Div.* **1969**, *95*, 758–761, doi:10.1061/JYCEAJ.0002065.
18. Cappelaere, B. Accurate Diffusive Wave Routing. *J. Hydraul. Eng.* **1997**, *123*, 174–181, doi:10.1061/(ASCE)0733-9429(1997)123:3(174).
19. Caleffi, V.; Valiani, A.; Zanni, A. Finite Volume Method for Simulating Extreme Flood Events in Natural Channels. *Journal of Hydraulic Research* **2003**, *41*, 167–177, doi:10.1080/00221680309499959.
20. Zolghadr, M; Hashemi, M. R; Zomorodian, S. M. A. ASSESSMENT OF MIKE21 MODEL IN DAM AND DIKE-BREAK SIMULATION. *Iranian journal of science and technology: IJST, Transaction A. Science.* **2011**, *35*, 247–262.
21. Taylan, E.D.; Damçayırı, D. 2D Hydrodynamic Model for Flood Analysis in Kinikli Stream Basin (Tekirdağ, Türkiye). *Iran J Sci Technol Trans Civ Eng* **2024**, *48*, 2691–2707, doi:10.1007/s40996-023-01298-1.
22. Vojtek, M.; Vojteková, J. Fluvial Flood Inundation Modeling: A Comparative Assessment of 1D and 2D Hydraulic Approach Using MIKE+. *Water Resour Manage* **2026**, *40*, 24, doi:10.1007/s11269-025-04423-z.
23. Sun, Z.P.; Zhao, Z.H.; Liu, Z.J.; Wang, X.; Lian, H.D; Wang, Y.; Ren, Z.H. Numerical simulation analysis of backwater of river-crossing bridges congestion based on MIKE21. Journal of Water Resources & Water Engineering, **2022**, 33(6): 129-136. (In Chinese). doi: 10.11705/j.issn.1672-643X.2022.06.16.
24. Zhu, H.W.; Jin, J.F.; Li, Z. Y.; Qian, X.C.; Xu, X. Influence of Qiantang River Jiuxi embankment optimization on flood control and tide protection. South-to-North Water Transfers and Water Science&Technology,**2021**,19(2):385-392.(In Chinese).doi: 10.13476/j.cnki.nsbdqk.2021.0041.
25. Yang, H.Q., Xu, X., He, K. Experimental study on the impact of tidal overtopping in Jiuxi section of the Qiantang estuary. Journal of Waterway and Harbor, **2021,** 42(5): 603-608. (In Chinese).
26. Cheng, W.L.; Pan, C.H.; Wu, X.G. Two-and Three-dimensional Model Simulations of Tidal Bore in Qiantang River and their Difference Analysis. Chinese Journal of Hydrodynamics,**2023**,38(3):383-390. (In Chinese). doi:10.16076/j.cnki.cjhd.2023.03.007.
27. Qiu, Y.; Li, W.; Chen, F.; Hu, P.; Zhao, Z.; Zhang, Y.; Zeng, J.; He, Z. Hydrodynamics of the Qiantang Tidal Bore and Its Responses to Embankment, Morphology, and River Discharge. *Sustainability* **2025**, *17*, 7363, doi:10.3390/su17167363.
28. Li, G.; Zhu, H.; Jian, H.; Zha, W.; Wang, J.; Shu, Z.; Yao, S.; Han, H. A Combined Hydrodynamic Model and Deep Learning Method to Predict Water Level in Ungauged Rivers. *Journal of Hydrology* **2023**, *625*, 130025, doi:10.1016/j.jhydrol.2023.130025.
29. Syed, Z.; Choi, G.; Byeon, S. A Numerical Approach to Predict Water Levels in Ungauged Regions—Case Study of the Meghna River Estuary, Bangladesh. *Water* **2018**, *10*, 110, doi:10.3390/w10020110.
30. Safavi, S.; Shamsai, A.; Saghafian, B.; Bateni, S. Modeling Spatial Pattern of Salinity Using MIKE21 and Principal Component Analysis Technique in Urmia Lake. *Curr. World Environ* **2015**, *10*, 626–633, doi:10.12944/CWE.10.2.28.
31. LI, W. J. Pondering on Project Layout of Major Tributaries and Medium and Small River Harnessing. Yellow River, 2013, 35(7): 4-5, 8. (In Chinese). doi: 10.3969/j.issn.1000-1379.2013.07.002.
32. Williams, J.J.; Esteves, L.S. Guidance on Setup, Calibration, and Validation of Hydrodynamic, Wave, and Sediment Models for Shelf Seas and Estuaries. *Advances in Civil Engineering* **2017**, *2017*, 1–25, doi:10.1155/2017/5251902.

 doi:10.20944/preprints202603.0241.v1

33. Soulsby, R. *Dynamics of Marine Sands*; Emerald Publishing Limited, 1997; ISBN 978-0-7277-2584-4.
34. Chen, Z.; Zhou, J.; Chen, Q. Research and Application of the Calculation Method of River Roughness Coefficient with Vegetation. *Water* **2023**, *15*, 2638, doi:10.3390/w15142638.